Resistivity saturation in substitutionally disordered γ-$Fe_{80-x}Ni_xCr_{20}$ ($14 \leq x \leq 30$) alloys

T. K. Nath and A. K. Majumdar
Department of Physics, Indian Institute of Technology, Kanpur 208016, India
(Received 28 December 1994; revised manuscript received 29 October 1995)

A systematic study of the electrical resistivity (ρ) has been carried out between 10 and 600 K on substitutionally disordered γ-$Fe_{80-x}Ni_xCr_{20}$ ($14 \leq x \leq 30$) austenitic stainless steel alloys in different magnetic states. We observe in each alloy, irrespective of its low-temperature magnetic state, a strong deviation from linearity (DFL) of ρ which is an indication of resistivity saturation at high temperatures. The temperature coefficient of resistivity (TCR$=\rho^{-1}d\rho/dT$) vs ρ curves for all the alloys merge in the temperature range of 100 to 600 K. This behavior indicates that both thermal and compositional disorders are equally important in determining the resistivity saturation. We have examined several models and find that the parallel-resistor and the ion-displacement models are the most appropriate ones in explaining this DFL of ρ at high temperatures. At low temperatures, in the long-range ferromagnetic and antiferromagnetic as well as in the mixed-phase regimes, the contribution to resistivity from the electron-magnon scattering ($\sim T^2$) dominates. In the spin-glass regime there is an additional T^3 term arising from the electron-phonon scattering in the presence of an s-d interaction.

I. INTRODUCTION

Transport properties, especially the variation of the electrical resistivity with temperature in substitutionally disordered crystalline materials (with short electron mean free paths), are still of interest because of the lack of a complete understanding of the mechanisms involved despite intense theoretical efforts. In a disordered metallic alloy, the electrical transport mainly depends on $k_F l$, where l is the mean free path and k_F the Fermi wave number of the conduction electrons. The alloys in the dilute limit generally have $k_F l > 1$ and the electronic states remain extended (long mean free paths) throughout the sample.[1] It is assumed that in these alloys Mathiessen's rule holds, the various scattering frequencies are additive, and Boltzmann transport is still valid.

However, in the case of alloys in the strongly disordered limit with large values of electrical resistivity (with short electron mean free paths and $k_F l \sim 1$ which is the Ioffe-Regel[2] criterion), the simple Boltzmann transport breaks down. The universal Mooij correlation[3] has almost become a rule for such kinds of highly resistive crystalline or amorphous alloys, though large discrepancies are found in some cases. At very low temperatures quantum interference effects become important and as a consequence electron localization and electron-electron interactions (many-body effects) give quantum corrections to the conductivity of highly resistive alloys.[4] At high temperatures, on the other hand, the deviation from linearity (DFL) of the resistivity leads to the so-called ''resistivity saturation'' and violates the simple Mathiessen's rule as well as the Bloch-Grüneissen theory. This happens in the case of many highly resistive (strong-disorder limit) materials[5,6] as well as in d-band alloys (e.g., Nb_3Ge, Nb_3Sn, Nb_3Al, etc.) with intermediate-T_c and rare earth superconductors[7,8] (e.g., $Y_{5-x}Dy_xOs_4Ge_{10}$, $Sc_{5-x}Dy_xIr_4Si_{10}$, etc.). Over the years, despite a lot of effort to understand this phenomenon theoretically[9–15] and experimentally,[5–8,16–18] a quantitative, microscopic theory is still a distant goal.

In the case of highly disordered magnetic materials, especially the $3d$ transition-metal alloys, the situation is much more complex. This is due to the presence of additional scattering mechanisms of magnetic origin. However, there are some extensive studies of electrical transport on noble-metal–transition-metal alloys (e.g., AuFe,[19] CuMn,[20] AuCr, AuMn, etc.) in the spin-glass (SG), mictomagnetic, or cluster glass and the long-range ferromagnetic (FM) or antiferromagnetic (AFM) phases which exist beyond the Kondo or dilute noninteracting regime. Sufficient attempts have been made to find out the nature of impurity scattering due to magnetic ions in noble-metal hosts for the entire regime. Despite a number of studies of electrical transport in transition-metal–transition-metal alloys (e.g., CrFe, NiMn,[21] NiMnPt,[22] CrMn, CrMnV, etc.), a concrete picture of the magnetic contribution to the resistivity is yet to emerge.

In this work we have performed systematic measurements of the electrical resistivity [$\rho(T)$] in the temperature range of 10–600 K of γ-$Fe_{80-x}Ni_xCr_{20}$ ($14 \leq x \leq 30$) highly resistive, concentrated magnetic austenitic stainless steel alloys in the fcc γ phase. The magnetic phase diagram[23,24] had been established in this alloy system through dc-magnetization, magnetic neutron scattering and ac-susceptibility measurements. Due to the competing exchange interaction (in the model of Heisenberg exchange) between different kinds of magnetic atoms (the nearest neighbor interaction is either FM or AFM with positive or negative values of the exchange integral J_{ij}), this system of alloys undergoes a compositional phase transition from long-range AFM ($x = 10$–14) to SG (17–21), to mixed FM and SG (23–26), to long-range FM ($x \geq 30$) order within the same crystallographic γ phase. In the mixed-phase alloys ($x = 23$–26), the coexistence of long-range FM and SG ordering was confirmed through M-H (Refs. 23,25) and magnetoresistance[25] measurements. This is in agreement with the Gabay-Toulouse[26] model of mixed phase where the transverse spin freezing (say, in the X-Y plane) takes place along with long-range FM ordering (in the Z direction) below the second transition.

We have earlier reported[25] magnetoresistance (MR) measurements on these alloys where we found that the MR are

negative until a temperature as high as 50 K in the field range of 0–1.7 T. A correlation between magnetization (M) and magnetoresistance ($\Delta\rho/\rho$) was observed only in the SG alloys ($x=19,21$) with $\Delta\rho/\rho \propto M^{2.5}$. $\rho(T)$ measurements on this system of alloys at low temperatures have been recently reported by Banerjee and Raychaudhuri.[27,28] They have found a resistivity minimum in each alloy[27] around the temperature 8–10 K. The low-temperature rise in $\rho(T)$ below $T_{\min}$ in each alloy has $\sqrt{T}$-like functional dependence which has been ascribed to an electron-electron interaction in the presence of weak localization. They also concluded that the magnetic state does not play any significant role in the $\sqrt{T}$ behavior which is due to quantum interference effects. In the temperature range $T_{\min}<T<80$ K,[28] they have found contributions to $\rho(T)$ from T^2 and T^3-dependent terms, their relative proportion being dependent on the Ni concentration.

The motivation behind the present work is to study the electrical transport properties of γ-$Fe_{80-x}Ni_xCr_{20}$ ($14 \leqslant x \leqslant 30$) alloys with varying magnetic phases within the *same* crystallographic fcc phase over a wider range of temperatures (10–600 K). At very high temperatures where the contribution to resistivity from magnetic scattering can be neglected, the deviation from linearity (DFL) of resistivity which might lead to saturation gives one an opportunity to thoroughly investigate this long-debated phenomenon for highly resistive crystalline magnetic alloys. Several models or theories have been proposed for the DFL of resistivity which ultimately lead to a saturation value. In the present work, we have considered some of them which are the most appropriate ones to explain this phenomenon and tested them rigorously with our $\rho(T)$ data at high temperatures. The role of magnetic ordering in the electronic transport has also been examined since these alloys are near the percolation threshold or the critical regime.

II. THEORY

It is very difficult to provide an exact theoretical description of the temperature dependence of the resistivity of the alloys under investigation since no theory has been developed so far which can describe the band structure as well as the spin structure of these kinds of 3d transition-metal alloys. In concentrated disordered magnetic alloys, the electron transport is much more difficult to understand because of the involvement of a large number of complicated scattering mechanisms. Therefore, the validity of Matthiessen's rule as well as the theory of classical Boltzmann transport in highly resistive alloys could be questioned. In 3d transition metals and alloys scattering of the conduction s electrons by phonons and their interaction with magnetic spin system (spin-disorder resistivity) are the main sources of the temperature dependence of the resistivity.[29–31] Generally, in both these cases the scattering may take place within a single band (s-s) or may involve s-d transitions. One of the earliest proposals to account for the resistivity variation with temperature of transition metals due to electron-phonon scattering, in the presence of an s-d interaction, was made by Wilson.[32] This is given by

$$\rho_{s\text{-}d}(T)=B\left(\frac{T}{\Theta_D}\right)^3\int_0^{\Theta_D/T}\frac{z^3dz}{(e^z-1)(1-e^{-z})}, \qquad (1)$$

which goes as T^3 at low temperatures and as T above Θ_D. Thus, the temperature exponent at low temperatures can be expected to vary from 3 to 5 (in the case of the *Bloch-Grüneissen* formula) depending on the shape and location of the Fermi surface of the s and d bands. The exponent was found in various transition elements[33] to lie between 2.0 and 5.3.

Turov,[34] Kasuya,[35,36] Mannari,[37] and Goodings[38] have shown that the spin-wave treatment in the presence of s-s and s-d interactions can lead to a T^2 contribution to the spin-disorder resistivity (ρ_{mag}) at low temperatures for ferromagnetic metals. Based on the spin-wave dispersion relation $E_q=\mathscr{D}q^2$, Kasuya has given the following expression for the spin-disorder resistivity:

$$\rho_{\mathrm{mag}}(T)=\frac{\pi^3\mathscr{V}m\mathscr{G}_{s\text{-}d}^2}{8\mathscr{N}e^2\hbar E_F}(g-1)^2j\left(\frac{kT}{k_F^2\mathscr{D}}\right)^2, \qquad (2)$$

where $\mathscr{G}_{s\text{-}d}$ is a parameter which describes the strength of the s-d interaction, g the Landé g factor, j the total quantum number of each magnetic atom, E_F the Fermi energy of the conduction electrons, $\mathscr{D}$ the spin-wave stiffness constant, and $\mathscr{V}$ and $\mathscr{N}$ are the volume and the number of atoms in the crystal, respectively. A similar result was obtained using a slightly different method by Mannari.[37] He estimated ρ_{mag} for Ni and found excellent agreement with the measurements of White and Woods[33] for the case of Fe, Co, and Ni [where $\rho=(13–16)\times10^{-6}\ T^2\ \Omega$ cm] in the low-temperature range.

Besides Eqs. (1) and (2), electrical resistance in transition metals and alloys can also arise from the collisions of the s electrons with the charge fluctuations of the itinerant d electrons. Here a T^2-dependent contribution of nonmagnetic origin may appear in the resistivity in the low-temperature range as predicted by Baber.[39,40]

In these highly resistive alloys, the high-temperature DFL of resistivity, which is the signature of resistivity saturation, is an interesting topic to focus on. Cote and Meisel[9] proposed a model which is referred to as the ''phonon-ineffectiveness'' model to interpret this downward DFL of the resistivity in the case of highly resistive materials at high temperature. They obtained a limiting resistivity when the electron mean free path l is of the order of the interatomic spacing. Taking the Debye-Waller factor to be 1, the electrical resistivity is given by

$$\rho(T)=\rho(0)+\left[1-\frac{\rho(T)}{\rho_D}\right]CT, \qquad (3)$$

where $\rho(0)$ is the measured residual resistivity, C a constant, and ρ_D the saturation resistivity corresponding to $l=2\pi/q_D$, where q_D is the lower cutoff of the phonon wave number.

Fisk and Webb[5] observed this kind of DFL of resistivity in $A15$ superconductors (e.g., Nb_3Sn, Nb_3Sb, etc.). They used the term ''resistivity saturation'' in the case of highly resistive materials (50–150 $\mu\Omega$ cm) and interpreted this phenomenon qualitatively in terms of the attainability of the electron mean free path l to its lowest possible value in the strong-disorder limit. This can be of the order of the inter-

atomic spacing a of the material ($l \sim a$), according to the Mott[41] and Ioffe-Regel criteria[2] ($k_F l \sim 1$).

The most widely accepted model for the phenomenon of resistivity saturation in high-resistivity materials is the empirical ''parallel-resistor'' or ''shunt-resistor'' model first proposed by Wiesmann *et al.*[6] They argued that in a disordered material, in addition to the usual Boltzmann conduction channel, there is an extra nonclassical channel and these two act in parallel. The total resistivity $\rho(T)$ is given by

$$\frac{1}{\rho(T)} = \frac{1}{\rho_{\text{ideal}}(T)} + \frac{1}{\rho_{\text{sat}}}, \tag{4}$$

where

$$\rho_{\text{ideal}}(T) = \rho_{\text{ideal}}(0) + \rho_{\text{ph}}(T) \tag{5}$$

and

$$\rho_{\text{ideal}}(0) = \frac{\rho(0)\rho_{\text{sat}}}{\rho_{\text{sat}} - \rho(0)}. \tag{6}$$

Here ρ_{sat} is the maximum limiting resistivity which is assumed to be independent of temperature and $\rho(0)$ the measured residual resistivity at $T=0$ K. The $\rho_{\text{ph}}(T)$ term is due to an electron-phonon interaction, the form of which can be assumed to be either the Bloch-Grüneissen[29] formula or Eq. (1), depending upon the behavior of the system at low temperatures ($T \ll \Theta_D$). Irrespective of the form chosen above, $\rho_{\text{ph}}(T)$ varies linearly with temperature at high temperatures ($T \geqslant \Theta_D$). Several theories have been proposed to understand the physical origin of such a phenomenological shunt-resistor model. Notable among them are the work by Allen and co-workers,[10,11] Gurvitch,[13,14] and Laughlin.[12] Gurvitch argued that the statistical distribution of relaxation times must have a lower cutoff (τ_0) and averaging over such a distribution would result in the parallel-resistor model [Eq. (4)] considering the Ioffe-Regel[2] criterion. Gurvitch[14] had shown that for different high-resistive metallic systems which show resistivity saturation, the Ioffe-Regel parameter ($k_F l$) lies between 3 and 6 instead of 1 if one assumes $l \sim a$. In addition to that, the conductivities at saturation (σ_{sat}) of these alloys are much higher (10–30 times) as compared to Mott's[41] *minimum metallic conductivity* ($\sigma_{\min} = 0.026 e^2/\hbar a$) as seen in many metallic systems (e.g., metal oxides) closer to the metal-insulator (M-I) transition. This relation is given by

$$\sigma_{\text{sat}} = (3\pi^2 n)^{2/3} a^2 \sigma_{\min}, \tag{7}$$

where n is the density of electrons at the Fermi level and a is the interatomic spacing.

Recently Ron *et al.*[42] have suggested an entirely different kind of model considering the effects of displaced ions on the conduction electrons to describe the DFL of resistivity at high temperatures. They have shown that the phenomenon of resistivity saturation can arise from the fact that the average ion displacement, at high enough temperatures, can exceed the wavelength of the electronic wave functions, while being still much smaller than the interatomic spacing. In this model, the electronic wave functions are extended, but may have short-length oscillations. Also, even in the weak scattering regime ($k_F l \gg 1$), saturation sets in long before the Ioffe-Regel[2] criterion comes into play. They obtained an expression for resistivity of the form

$$\rho(T) = \rho_m - D T_0 \exp\left[\frac{T}{T_0}\right], \tag{8}$$

where T_0 is a characteristic temperature, D is a constant, and ρ_m is the saturation resistivity. This model is especially suitable for those transition metals whose orbitals possess a large number of lobes; namely, the distance between the zeros of the wave function is considerably smaller than the interatomic spacing.

III. EXPERIMENTAL DETAILS

The alloys γ-$Fe_{80-x}Ni_xCr_{20}$ with $x=14$, 19, 21, 23, 26, and 30 were prepared[23] by induction melting in an argon atmosphere from metals of at least 99.99% purity. The samples are cut into thin rectangular strips for resistivity measurements, homogenized at 1050 °C for 30 h in an argon atmosphere and then rapidly quenched to room temperature in brine. All the samples are characterized through the x-ray diffraction (XRD) method to investigate the possible presence of any second phase (say, of bcc structure) apart from the fcc γ phase. The diffraction patterns reveal that all the alloys have single-phase fcc structure similar to that of γ-Fe in the austenite state, with lattice parameter $a = (3.58 \pm 0.01)$ Å . There is a very small change in the lattice constant with concentration. The nominal chemical composition of the alloys was checked through scanning electron microscope (SEM) and energy dispersive x-ray analyses (EDAX). The analyzed compositions are found to be within 0.5% of the nominal ones for Ni and Cr.

The resistivity measurements are carried out using the standard four-probe dc technique employing a Datron Autocal digital (7 and 1/2 digit) multimeter (model 1071). The temperature of the samples is controlled and monitored by a Lake-Shore temperature controller (model DRC 93C). The electrical contacts to the sample are made with Zn-Cd nonsuperconducting solder using $ZnCl_2$ flux. A closed-cycle helium refrigerator (Cryosystems Inc.) is used in the temperature range of 10–370 K. A different setup is used for the resistivity measurements up to 600 K from above room temperature. The electrical connections are made by pressure contacts employing four high purity Ag wires (Oxford Instruments), avoiding the formation of any insulating oxide at high temperatures, thereby providing a better electrical contact. Highly resistive nichrome wire is used to wind the heater. The measurements are carried out in a big cylindrical quartz tube in the presence of a continuous flow of 1.5 psi argon gas.

The accuracy in resistance measurements is better than 1–5 parts in 10^5 in the low-temperature range, but at high temperatures, it is less by an order of magnitude. The stability of the temperature during the measurements is within ± 10 mK and ± 500 mK in the low- and high-temperature ranges, respectively. The absolute values of the resistivity are accurate only within $\pm 5\%$ due to uncertainties in the measurements of the dimensions of the samples.

The resistivity measurements are automated using an

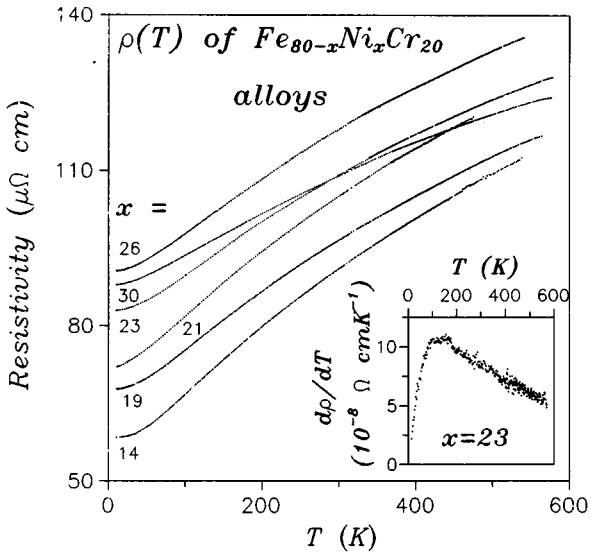

FIG. 1. Experimental $\rho(T)$ plot of $Fe_{80-x}Ni_xCr_{20}$ ($x=14$, 19, 21, 23, 26, and 30) highly resistive austenitic stainless steel alloys in the temperature range of 10–600 K. The inset shows a typical $d\rho/dT$ vs T plot for $x=23$.

IBM-compatible PC/AT through an IEEE-488 interface with the measuring instruments.

IV. RESULTS AND DISCUSSION

A. General features of the experimentally observed $\rho(T)$

In Fig. 1 we have shown the experimentally observed resistivity $\rho(T)$ data in the temperature range of 10–600 K for the six disordered magnetic alloys of γ-$Fe_{80-x}Ni_xCr_{20}(14\leqslant x\leqslant 30)$, all of which are around the stainless steel composition in the austenite state. The inset of Fig. 1 shows a typical behavior ($x=23$) of the temperature dependence of $d\rho/dT$ of these alloys. From these $\rho(T)$ curves the following observations can be made.

(i) There is no distinct signature of a magnetic transition (FM, mixed phase, SG, or AFM) in the $\rho(T)$ plots at the respective transition temperatures (T_c, T_{SG}, or T_N) listed in Table I.

(ii) There is a peak in $d\rho/dT$ for each alloy at around 100 K as shown in the inset of Fig. 1.

(iii) $\rho(T)$ of each alloy varies faster than $T(\sim T^2)$ until 50–60 K.

(iv) The $\rho(T)$ curve for each alloy starts deviating from linearity in the downward direction roughly beyond 200 K ($\approx\Theta_D/2$). This behavior is manifested in the $d\rho/dT$ curve as well, where it starts to fall significantly from the maximum value. However, in sharp contrast to these results, Banerjee and Raychaudhuri[28] have observed that above 100 K, the $\rho(T)$ plot for each alloy is linear until 300 K (their highest temperature of measurements). There is no indication of any saturation effect even at 300 K.

In Table I we have shown the different magnetic transition temperatures (T_c, T_{SG}, and T_N) taken from Ref. 23 and ρ(10 K), ρ(300 K), and the temperature coefficient of resistance (TCR$=\rho^{-1}d\rho/dT$) at 300 and 500 K from the data of Fig. 1 for the alloys under investigation. From Table I one observes that all these disordered concentrated magnetic alloys possess very high values of residual resistivity [ρ(10 K)]. The TCR of each alloy is very small at 300 K and becomes still smaller at 500 K. It is also noticed that the magnitude of the TCR at room temperature decreases with ρ(300 K) for varying alloy compositions, thus obeying Mooij criterion.[3] Figure 2 shows the variation of the percentage change of ρ(500 K) with respect to ρ(10 K) and ρ(200 K) with an increase of Ni concentration (x). It shows a roughly linear dependence. The percentage change of ρ(500 K) becomes smaller on the high-Ni-concentration side with large values of the residual resistivity. The inset of Fig. 2 shows an increase of the residual resistivity ρ(10 K) with Ni concentration (x) until $x\approx 27$.

Figure 3 is a plot of TCR vs x at three temperatures (100, 300, and 500 K). At each temperature the best-fitted curve shows a linear dependence of TCR on x. The slopes of the best-fitted straight lines as well as the TCR gradually decrease with temperature and both have a tendency to become zero beyond a certain temperature when the best-fitted line coincides with the x axis. This implies saturation of the resistivity beyond a certain temperature.

Figure 4 shows a very striking correlation in these highly resistive alloys. It reveals that the thermal and compositional disorders have similar effects on the resistivity saturation. This is a plot of TCR with ρ for all the alloys as well as for

TABLE I. Ni concentration (x) dependence of magnetic transition temperatures (T_c, T_{SG}, T_N taken from Ref. 23, resistivities ρ at 10 and 300 K, and TCR $\rho^{-1}(d\rho/dT)$ at 300 and 500 K of γ-$Fe_{80-x}Ni_xCr_{20}(14\leqslant x\leqslant 30)$ alloys.

Ni x (at.%)	T_c (K)	T_{SG} (K)	T_N (K)	$\rho_{10\,K}$ ($\mu\Omega$ cm)	$\rho_{300\,K}$ ($\mu\Omega$ cm)	$[\rho^{-1}(d\rho/dT)]300$ K ($\times10^{-4}$/K)	$[\rho^{-1}(d\rho/dT)]500$ K ($\times10^{-4}$/K)
14			26	58.4	91.0	11.5	7.5
19		12		67.8	96.6	9.3	6.5
21		10		72.1	105.1	9.3	6.0
23	35	20		83.0	109.0	7.8	5.5
26	56	7		90.6	118.3	7.6	5.2
30	135			87.9	109.0	6.5	4.1

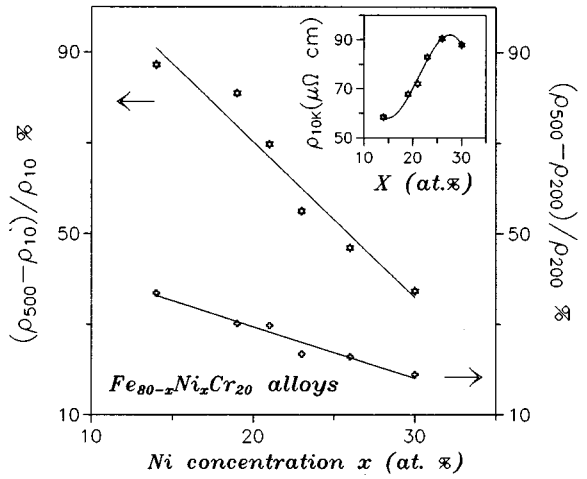

FIG. 2. Percentage change of resistivity ρ(500 K) relative to ρ(10 K) and ρ(200 K) of $Fe_{80-x}Ni_xCr_{20}$ ($14 \leqslant x \leqslant 30$) alloys as a function of Ni concentration (x). The inset shows the x dependence of the residual resistivity [ρ(10 K)]. The solid curve in the inset is just a guide to the eye.

the whole range of temperature beyond 100 K. Here the increase of ρ at a fixed temperature implies increase in the compositional or chemical disorder. At the same time, the increase of temperature for a particular alloy corresponds to an increase in the thermal disorder. Surprisingly, for all the six alloys in the temperature range beyond 100 K, the data points fall on a common curve, no matter what causes the change of resistivity, compositional disorder or thermal disorder. As the disorder is increased (compositional or thermal), the TCR (α) decreases gradually. We have fitted this curve to an empirical relation $\alpha = -(\gamma/\rho) + \delta$, where γ and δ are constants ($\chi^2 \approx 10^{-7}$). By extrapolation of this best-fitted curve to TCR (α)=0 where it cuts the ρ axis, we have estimated the value of saturation resistivity as

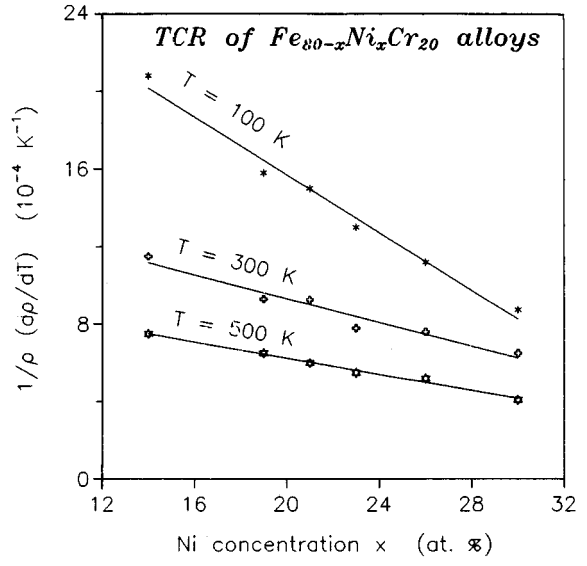

FIG. 3. Ni concentration (x) dependence of the temperature coefficient of resistivity (TCR=$\rho^{-1}d\rho/dT$) of $Fe_{80-x}Ni_xCr_{20}$ ($14 \leqslant x \leqslant 30$) alloys at 100 K, 300 K, and 500 K.

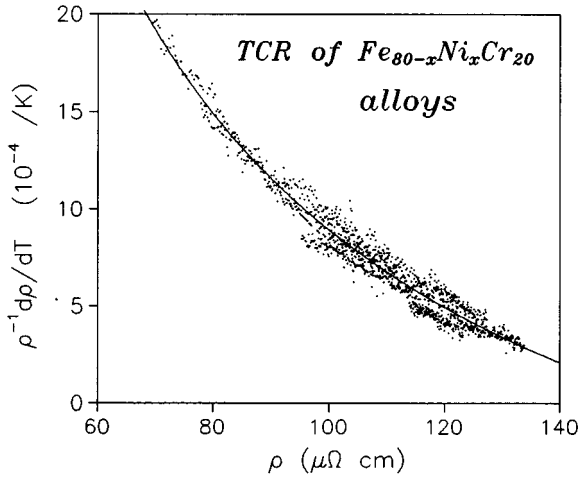

FIG. 4. Resistivity (ρ which results from either thermal or compositional disorder) dependence of the TCR of $Fe_{80-x}Ni_xCr_{20}$ ($14 \leqslant x \leqslant 30$) alloys in the temperature range beyond 100 K. The solid line is the best-fitted curve.

$\rho_{sat} \approx 180\mu\Omega$ cm. This kind of correlation has also been found recently in crystalline TiAl alloys.[18]

B. Analysis of ρ(T) data in the temperature range T_{min} ($\approx$10 K)$\leqslant T \leqslant$70 K ($\approx\Theta_D/5$)

We have tried to fit the observed $\rho(T)$ data of each alloy to a single temperature-dependent term bT^n along with a constant term a in the temperature range of 10–60 K. The fit functions, the values of the fitting parameters, the ranges of temperature, and the values of χ^2, which give the goodness of fit, for all the six alloys are listed in Table II. χ^2 is defined as

$$\chi^2 = \frac{1}{N}\sum_{i=1}^{i=N}\left(\frac{\rho^i_{expt}-\rho^i_{fit}}{\rho^i_{expt}}\right)^2,$$

where N is the number of data points. From Table II the following observations can be made.

(1) For the alloy with $x=14$ which has a single PM-AFM transition[23] with $T_N=26$ K, the data fit very well with the function $a+bT^2$ in the low-temperature range of 10–60 K beyond which the fit becomes poor. However, between 10 and 60 K, $\chi^2 \approx 10^{-8}$ and is consistent with the experimental accuracy. We have shown the experimental data and the best-fitted curve in Fig. 5 which is a plot of ρ vs T^2 for the alloy with $x=14$. The figure shows a clear linear dependence in the low-temperature range. The inset of Fig. 5 shows the percentage deviation of the experimental data from the best-fitted values as a function of temperature.

(2) For the alloys with $x=19$ and 21, which have PM-SG transitions[23] at around 12 and 10 K, respectively, an additional T^3 term is necessary along with the T^2 term between 10 and 50 K to make the χ^2 ($\approx 10^{-8}$) consistent with the experimental accuracy. The experimental data and the best-fitted curves are shown in Fig. 6 for the spin-glass alloys ($x=19$ and 21).

TABLE II. Fitting parameters for the $\rho(T)$ data to different fit functions, low-temeprature ranges, and the values of χ^2 (defined in text) for γ-$Fe_{80-x}Ni_xCr_{20}$($14 \leq x \leq 30$) alloys.

Ni x (at. %)	Fit function	Fit range (K)	a ($\mu\Omega$ cm)	b ($10^{-3}\mu\Omega$ cm K^{-2})	c ($10^{-6}\mu\Omega$ cm K^{-3})	χ^2 (10^{-8})
14	$a+bT^2$	10–60	58.3	1.01		2.9
19	$a+bT^2+cT^3$	10–50	67.8	0.39	7.5	6.1
21	$a+bT^2+cT^3$	10–50	72.0	0.74	2.1	0.4
23	$a+bT^2$	10–40	82.9	1.07		3.9
26	$a+bT^2$	10–50	90.5	0.94		3.7
30	$a+bT^2$	10–50	87.8	0.99		1.6

(3) For the alloys with $x=23$ and 26 which are in the mixed phase having T_c and T_{SG} at 35, 20, and 56, 7 K, respectively, the function $a+bT^2$ again, in the low-temperature region, fits very well. This fit is as good as in the earlier alloys.

(4) For the alloy with $x=30$, which has only a PM-FM transition[23] at 135 K, the fit function $a+bT^2$ seems to be the correct choice, giving a $\chi^2 \approx 10^{-8}$ between 10 and 50 K. The experimental data along with the best-fitted curves for $x=23$, 26, and 30 are shown in Fig. 7, where ρ is plotted against T^2. These curves show a clear linear dependence in the low-temperature region.

Figure 8 shows how the fitting parameters, namely, the constant term a and the coefficient of the T^2 term b, vary with the increase of Ni concentration (x). The constant a, which can be attributed to the residual resistivity of these alloys, increases with x and has a peak at around $x=27$ (percolation threshold ≈ 20 at. % of Ni). Thus its behavior is very similar to that of $\rho(10\ \mathrm{K})$ as shown earlier in the inset of Fig. 2. The coefficient b has a large value for $x=14$. It has a minimum near $x=19$ and then it regains its large value around $x=23$–30 at. % of Ni. From these observations, it appears that the T^2 contribution dominates for the alloys which are away from the spin-glass region ($x=17$–21) and in which long-range (FM or AFM) magnetic ordering sets in. Here the value of b is more or less constant ($\approx 1\times10^{-3}\mu\Omega$ cm K^{-2}).

The T^3 contribution appears only in alloys with $x=19$ and 21 which are in the spin-glass phase at the lowest temperature. In these alloys the T^2 contribution is somewhat small as compared to those of the others.

In these concentrated magnetic alloys, the appearance of a T^2 contribution to ρ at low temperatures cannot be attributed directly to a single mechanism. If we compare the T^2 contribution to ρ of these alloys with those in pure Fe, Ni, and Co, as investigated by White and Woods,[33] we find that $b \approx (0.4\text{–}1.1)\times10^{-3}\mu\Omega$ cm K^{-2} in the present case which is one to two orders of magnitude higher than those in pure Fe, Ni, or Co [$\approx (1.3\text{–}1.6)\times10^{-5}\mu\Omega$ cm K^{-2}] and the one calculated by Baber.[39,40] Thus the T^2 contribution due to the Baber mechanism is too small to explain our results.

Next we attempt to explain this T^2 dependence of ρ in the

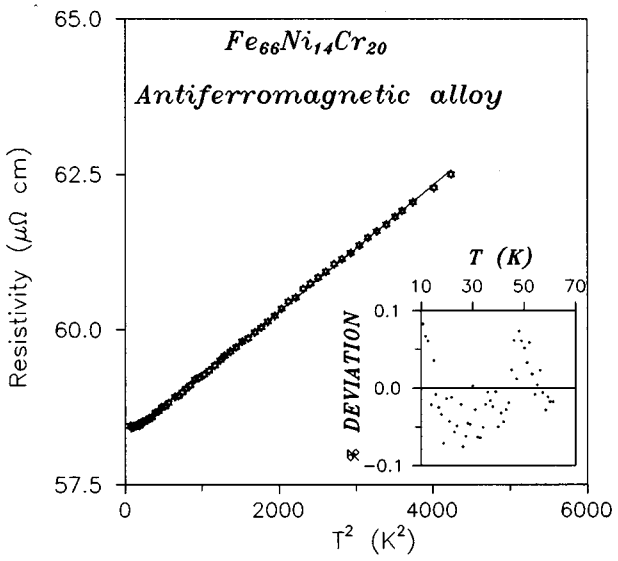

FIG. 5. Resistivity (ρ) vs T^2 plot of $Fe_{66}Ni_{14}Cr_{20}$ antiferromagnetic alloy in the temperature range of 10–60 K. The solid line is the best-fitted curve. The inset plots the percentage deviation of the fit from the experimental data.

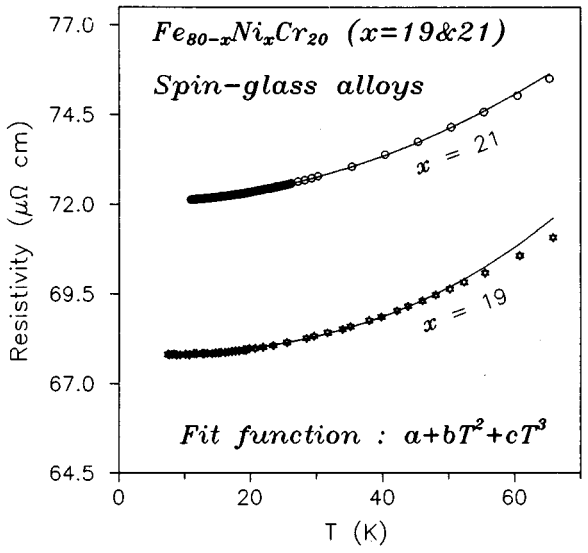

FIG. 6. Temperature dependence of resistivity of $Fe_{80-x}Ni_xCr_{20}$ ($x=19$ and 21) spin-glass alloys in the low-temperature range. The solid lines are the best-fitted curves for the function $a+bT^2+cT^3$.

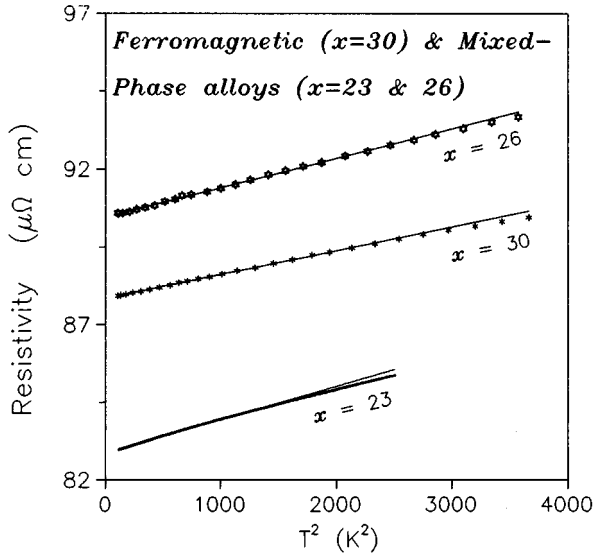

FIG. 7. ρ vs T^2 plots of $Fe_{50}Ni_{30}Cr_{20}$ ferromagnetic and $Fe_{80-x}Ni_xCr_{20}$ ($x=23$ and 26) mixed-phase alloys in the low-temperature range. The solid lines are the best-fitted curves.

light of the electron-magnon (spin-wave) scattering mechanism which seems to be the most plausible one. It also provides a rather consistent picture. It is clear that for the alloys in the long-range FM ($x=30$) or AFM ($x=14$) regimes as well as those in the mixed-phase ($x=23$ and 26) regime where the long-range magnetic ordering starts appearing, the T^2 contribution could be very large. In the case of the alloys ($x=19$ and 21) in the SG regime, the T^2 contribution drops down and the appearance of the extra T^3 term can be linked with electron-phonon scattering in the presence of an s-d interaction [Eq. (1)] in the transition metals.

We can, in principle, estimate the spin-disorder resistivity ($\rho_{\rm mag}$) in these alloys theoretically in the light of the spin-wave theory using Eq. (2). Unfortunately, there is no information on the spin-wave stiffness constant ($\mathscr{D}$) and the strength of the s-d interaction ($\mathscr{G}_{s\text{-}d}$) for these magnetic alloys as no band theory calculation has been developed for this system of alloys so far. Thus it is not possible to estimate $\rho_{\rm mag}$ quantitatively at the present stage.

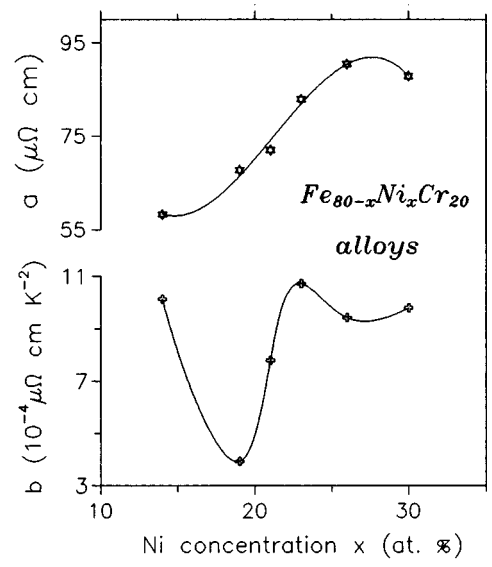

FIG. 8. Ni concentration (x) dependence of the fit parameters a and b of $Fe_{80-x}Ni_xCr_{20}$ ($14 \leqslant x \leqslant 30$) alloys in the low-temperature range. The solid lines are just guides to the eye.

When we compare our findings with those of Banerjee and Raychaudhuri[28] we find that there is an excellent qualitative agreement at low temperatures. However, some minor differences exist; e.g., for the long-range or mixed-phase ordering ($x=14$, 23, 26, and 30) the contribution of the T^3 term is about 1% of that of the T^2 term in their work whereas it is smaller than 0.1% in the present case. Although the experimental resolution is about the same, the fact that the values of χ^2 are much less in our studies in comparison to theirs ($\chi^2 \approx 10^{-8}$ and 10^{-6}, respectively) implies that the fit of our $\rho(T)$ data to various functions is better.

C. Analysis of $\rho(T)$ data in the temperature range $200\ (\approx\Theta_D/2) \leqslant T \leqslant 600$ K

From Fig. 1, which shows $\rho(T)$ of all the alloys under investigation, it is obvious that each curve shows a strong downward deviation from linearity (DFL) at high temperatures and also a tendency towards saturation at still higher temperatures. This DFL of ρ at high temperatures obviously cannot be linked with any kind of correlated magnetic spin scattering as the magnetic transition temperatures[23] are very low, ruling out any magnetic origin of the DFL. We have attempted to explain this behavior of $\rho(T)$ in the light of various models mentioned in Sec. II.

Obviously $\rho(T)$ at high temperatures is not consistent with that predicted by a simple electron-phonon scattering theory, viz., $\rho(T)\sim T$ as in the Bloch-Grüneissen[29] formula and Eq. (1) (Wilson). Therefore, we have fitted our data to the ''phonon-ineffectiveness'' model predicted by Cote and Meisel[9] [Eq. (3)] in the temperature range of 200–600 K. However, it is found that the fits in all the alloys are very poor ($\chi^2 \approx 10^{-4}$) in comparison with the experimental accuracy. As a consequence, we rule out the validity of this model in this system of alloys.

We have also fitted the high-temperature $\rho(T)$ data to Eq. (4) which is obtained from the widely accepted ''parallel-resistor'' model. The form of $\rho_{\rm ph}$(T) that we have chosen is contained in Eq. (1). This arises due to the phonon-assisted s-d scattering as proposed by Wilson[32] for transition metals. Since the exponents of T of the observed $\rho(T)$ in the low-temperature range are small (2–3) for this system of magnetic $3d$ transition-metal alloys, the use of Eq. (1) (Wilson) instead of the Bloch-Grüneissen formula is justified although both are of the same form at high temperatures ($\rho \propto T, T \geqslant \Theta_D$). We have abbreviated $\rho_{\rm ideal}(0)=\varepsilon$ which is a temperature-independent constant.

The value of the Debye temperature (Θ_D) used in Eq. (1) is $\approx$ 400 K, as obtained from the specific heat measurements reported by Pecherskaya *et al.*,[43] falling in the range of 370–400 K. No appreciable change in the quality of fit (χ^2) is observed as we vary Θ_D between 370 and 400 K. Recently, from a thorough investigation of the resistivity saturation of $Ti_{1-x}Al_x$ ($x \leqslant 0.135$) disordered alloys by Lin and co-workers,[18,44] it was concluded that a single value of

TABLE III. Ni concentration (x) dependence of the fitting parameters for the $\rho(T)$ data to Eq. (4) of the parallel-resistor model and the values of χ^2. The range of fit is taken betwen 200 and 600 K for the $Fe_{80-x}Ni_xCr_{20}(14 \leq x \leq 30)$ alloys.

Ni x (at. %)	$\varepsilon[=\rho_{ideal}(0)]$ ($\mu\Omega$ cm)	B ($10^{-4}\Omega$ cm)	ρ_{sat} ($\mu\Omega$ cm)	χ^2 (10^{-7})
14	66.2	2.0	252.7	5.9
19	85.0	2.1	234.1	3.4
21	92.1	2.8	225.0	2.8
23	117.6	3.1	205.8	1.4
26	131.8	3.1	223.7	5.1
30	142.5	3.4	183.0	3.0

ρ_{sat} cannot describe the resistivity saturation for the entire range of x. Also a proper choice of the range of fit made the quality of fit much better as well as the fitting parameters more meaningful in their case.

Along the same lines, here we have kept ρ_{sat}, a free adjustable fitting parameter along with ε [$\approx\rho_{ideal}(0)$] and B [in Eqs. (4), (5), and (1)]. The range of fit is selected within 200 ($\approx\Theta_D/2$)–600 K for all the alloys. We have evaluated the integral of Eq. (1) numerically using the DO1AHF (one-dimensional quadrature, adaptive, finite interval, and strategy due to Patterson) NAG routine which is suitable for any well-behaved function. A nonlinear least-squares approach is employed for fitting the experimental $\rho(T)$ data to Eq. (4) (parallel-resistor model). In Table III we have listed all the fitting parameters, namely, ε, B, and ρ_{sat} and the values of χ^2 for the six γ-$Fe_{80-x}Ni_xCr_{20}$ ($14 \leq x \leq 30$) alloys.

Figure 9 shows the experimental $\rho(T)$ data (dots) along with the best-fitted curves [solid line using Eq. (4)] for the alloys with $x=23$, 26, and 30 in the temperature range of 200–600 K. The excellent quality of fit is obvious from the indistinguishability between the data and the best-fitted curves. The inset of Fig. 9 shows the temperature dependence of a typical percentage deviation of the data ($x=23$) from the best-fitted values. Figure 10 is the same as Fig. 9 except that it is for the samples with $x=14$, 19, and 21. In the inset of Fig. 10 we have shown a typical likelihood distribution of the relative errors $P(\Delta\rho/\rho)$ for these kinds of fits for $x=19$. Generally, for a perfect fit and negligible experimental error (ideal condition), one gets a very narrow peak, centered around $\Delta\rho/\rho=0$. This follows a Gaussian-like (normal) distribution. However, in our case, the plot has some spread with secondary maxima which appear at both the positive and negative sides of $\Delta\rho/\rho=0$. We have drawn a smooth curve which follows a Gaussian-like distribution with a peak at $\Delta\rho/\rho=0$ and a full width at half maximum (FWHM) $\approx 4 \times 10^{-4}$. We have mentioned in Sec. III that the accuracy of our experimental data at the higher temperatures is about 5 parts in 10^4. So the FWHM resulting from this kind of fitting procedure and the order of χ^2 ($\approx 10^{-7}$) given in Table III are clearly of the same order as the experimental accuracy. The high quality of this fit indicates that the parallel-resistor model can reproduce reasonably well the saturation behavior of ρ in our γ-$Fe_{80-x}Ni_xCr_{20}$ alloys at high temperatures.

From Table III we observe that (i) the values of the parameter ε [$\rho_{ideal}(0)$ of Eq. (5)] increase with Ni concentration (x) (shown in Fig. 11), (ii) the parameter B, which is the strength of the Bloch-Wilson electron-phonon interaction in the presence of the s-d scattering term, increases [(2.0–3.4) $\times 10^{-4}\Omega$ cm] with Ni concentration (x) (shown in Fig. 11), and (iii) the saturation values of the resistivity, ρ_{sat}, differ [(183–253) $\mu\Omega$ cm] from each other for various alloys. The inset of Fig. 11 shows the concentration (x) dependence of ρ_{sat}.

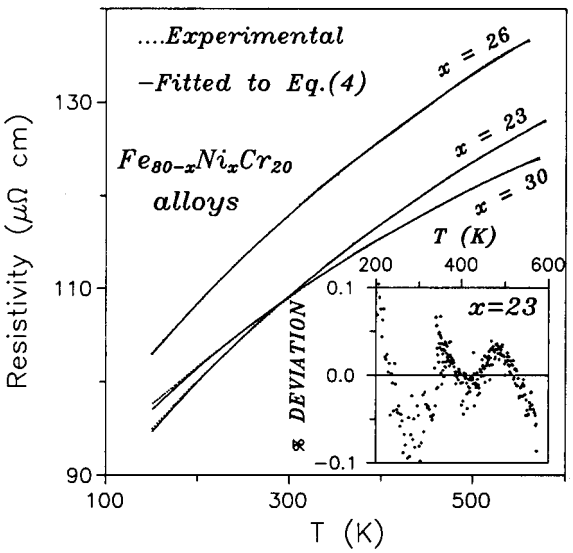

FIG. 9. Experimental (dots) ρ vs T plots of $Fe_{80-x}Ni_xCr_{20}$ ($x=23$, 26, and 30) alloys in the temperature range of 150–600 K. The best-fitted curves (solid lines) for the alloys are plotted using Eq. (4) (parallel-resistor model). The inset plots the temperature dependence of a typical percentage deviation of fit for $x=23$.

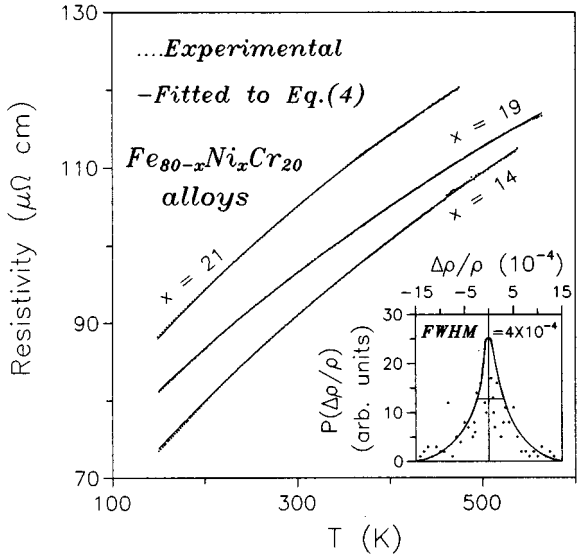

FIG. 10. Experimental (dots) ρ vs T plots of $Fe_{80-x}Ni_xCr_{20}$ ($x=14$, 19, and 21) alloys in the temperature range of 150–600 K. The best-fitted curves (solid lines) for the alloys are plotted using Eq. (4) (parallel-resistor model). The inset plots a typical likelihood distribution of the relative errors [$P\Delta\rho/\rho$] of the fit for $x=19$.

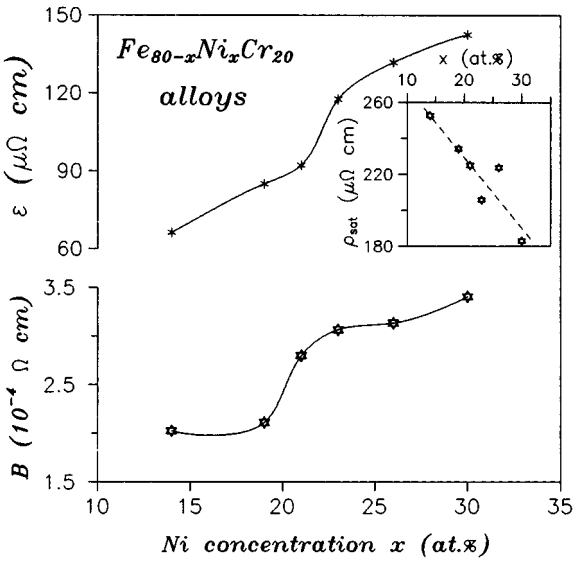

FIG. 11. Ni concentration (x) dependence of the fitting parameters ε and B of Eq. (4) (parallel-resistor model) of $Fe_{80-x}Ni_xCr_{20}$ ($14 \leqslant x \leqslant 30$) alloys. The solid lines are just guides to the eye.

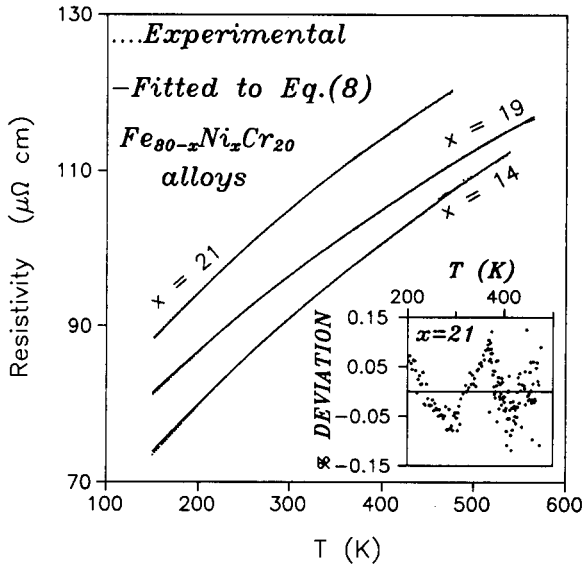

FIG. 12. Experimental (dots) ρ vs T plots along with the best-fitted curves (solid lines) using Eq. (8) (ion-displacement model) in the temperature of 200–600 K of $Fe_{80-x}Ni_xCr_{20}$ ($x=23$, 26, and 30) alloys. The inset plots the temperature dependence of a typical percentage deviation of the fit for $x=23$.

Whether the values of these fitting parameters are physically meaningful has to be seen. Using Eq. (6) and the fitted parameters ϵ [$=\rho_{\text{ideal}}(0)$] and ρ_{sat}, we have obtained values of $\rho(0)$ which are within 10% of our measured $\rho(10\text{ K})$ for all the alloys. Also, the strength of the Bloch-Wilson interaction term B is enhanced with the increase of Ni concentration (x) at the cost of Fe. This may be attributed to the enhancement of the electron-phonon scattering due to possible changes in the density of the d states at the Fermi level. The values of ρ_{sat} decrease roughly linearly with Ni concentration. If we assume a single value of ρ_{sat} with some fluctuations, then on averaging the best-fitted values for all the alloys we get $\rho_{\text{sat}} \approx (220 \pm 30)\ \mu\Omega$ cm. However, the validity of having a single value of ρ_{sat} for the entire concentration (x) is not very clear. Some of the experimental results[18,44] support multiple values of ρ_{sat} for a range of concentrations.

We have also examined our experimental data in the light of the ion-displacement model of Ron *et al.*[42] through nonlinear least-squares fits to Eq. (8). We have kept ρ_m, D, and T_0 as adjustable parameters in the range of 200–600 K. Figure 12 plots the experimental data (dots) and the best-fitted curves (solid lines) for alloys with $x=23$, 26, and 30. The typical percentage deviation is shown in the inset of Fig. 12 for $x=23$. Figure 13 and its inset are the same as Fig. 12 except that they are for $x=14$, 19, and 21 alloys and the inset is for $x=21$. We have summarized in Table IV the values of the fitting parameters ρ_m, D, and T_0 as well as the values of χ^2 obtained from fitting the data to Eq. (8). The following features can be observed from the table.

(i) No unique value of the saturation resistivity (ρ_m) is found, very much like the earlier case of the parallel-resistor model. ρ_m varies from 148 to 176 $\mu\Omega$ cm in these alloys. The range of this ρ_m is smaller than that of ρ_{sat} [(183–253) $\mu\Omega$ cm] as found from the parallel-resistor model. In the inset of Fig. 14 we have shown the comparative plots of ρ_m and ρ_{sat} as a function of $\rho(10\text{ K})$ for all the alloys. The nature of both the plots is more or less similar though their absolute values differ.

(ii) The values of the electron-phonon scattering coefficient D lie between 0.12 and 0.16 $\mu\Omega$ cm K^{-1}.

(iii) The fitted values of the characteristic temperature T_0 decrease monotonically from $\approx$ 825 to 600 K as the Ni

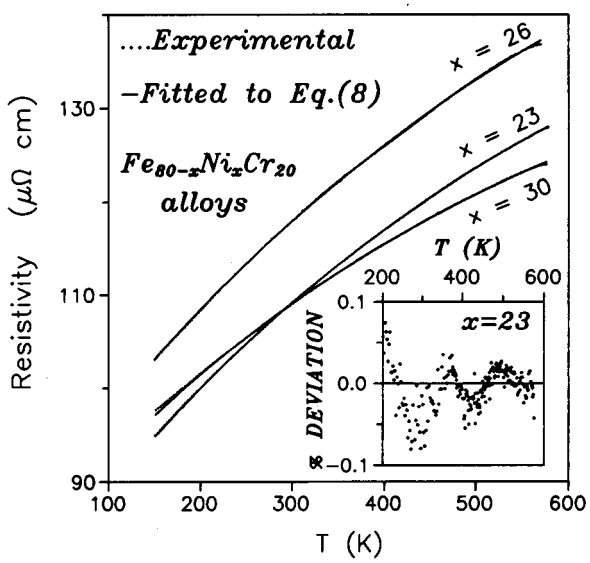

FIG. 13. Experimental (dots) ρ vs T plots along with the best-fitted curves (solid lines) using Eq. (8) in the temperature range of 200–600 K of $Fe_{80-x}Ni_xCr_{20}$ ($x=14$, 19, and 21) alloys. The inset plots the temperature dependence of a typical percentage deviation of the fit for $x=21$.

TABLE IV. Fitting parameters for the $\rho(T)$ data to Eq. (8) of the ion-displacement model and the values of χ^2. The range of fit is taken within 200–600 K for γ-$Fe_{80-x}Ni_xCr_{20}$($14 \leqslant x \leqslant 30$) alloys.

Ni x (at. %)	ρ_m ($\mu\Omega$ cm)	D ($\mu\Omega$ cm K^{-1})	T_0 (K)	χ^2 (10^{-7})
14	176.3	0.149	823.0	7.9
19	168.4	0.133	786.9	3.6
21	165.8	0.163	608.7	2.5
23	160.3	0.139	603.8	8.3
26	174.7	0.139	648.6	6.1
30	147.9	0.119	557.7	1.9

concentration (x) and ρ(10 K) increase. This is shown in Fig. 14. Equation (8) of the ion-displacement model can be written as

$$\rho_m = \rho(0K) + DT_0, \tag{9}$$

putting $T=0$. T_0 is the characteristic temperature at which the average ion displacement first becomes comparable with the distance between the zeros of the electronic wave function. The form of Eq. (9) tells us that static and thermal disorders play equally important roles in determining the resistivity saturation.

(iv) The values of χ^2 range from 1.9 to 8.3 $\times$ 10^{-7} in these fits to the ion-displacement model [Eq. (8)] and are consistent with the experimental accuracy. The order of χ^2 as well as the percentage deviation indicate that the ion-displacement model is also a strong candidate which can explain our experimental high-temperature $\rho(T)$ data reasonably well.

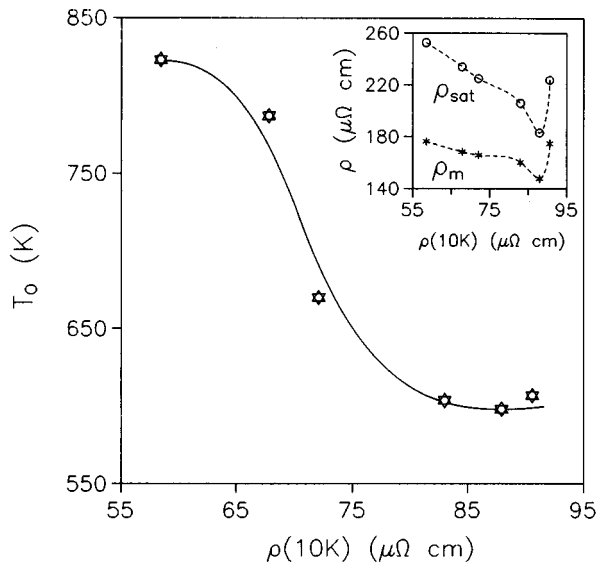

FIG. 14. Plot of the variation of T_0 with ρ (10 K) (experimental) for $Fe_{80-x}Ni_xCr_{20}$ ($14 \leqslant x \leqslant 30$) alloys. T_0 is the characteristic temperature in Eq. (8) of the ion-displacement model. The inset shows the comparative variation of ρ_m and ρ_{sat} [from Eqs. (8) and (4), respectively) with Ni concentration (x). The dashed lines are just guides to the eye.

Mott and others[41] calculated the saturation value of resistivity ρ_{sat} using the Kubo-Greenwood formula with the condition that the electron mean free path is as small as the lattice spacing ($l \sim a$) in the strong-disorder limit and found that

$$\sigma_{sat} = \rho_{sat}^{-1} = (0.33e^2/\hbar a). \tag{10}$$

Mott also claimed that a similar result like that of Eq. (10) can be found from the Boltzmann formula assuming spherical Fermi surface (free electron model). Gurvitch[13] had generalized the form of Eq. (10) considering α free electrons per cubic cell a^3 and wrote a modified relation

$$\sigma_{sat} = 0.33\alpha^{2/3}e^2/\hbar a \tag{11}$$

or

$$\rho_{sat} = 1.29 \times 10^{18}/(n^{2/3}a), \tag{12}$$

where the electron concentration n is in cm^{-3} and the lattice spacing a is in Å. We have estimated ρ_{sat} in our alloys using the value of $n=(6–7) \times 10^{22}$ /cm^3, as found from the recent Hall effect measurements[45] at room temperature and the lattice spacing a of 3.58 Å obtained from our XRD measurements. Substituting these values in Eq. (12) we obtain $\rho_{sat} \approx 215$ $\mu\Omega$ cm. This is in excellent agreement with our average value of ρ_{sat} ($\approx$ 220 $\mu\Omega$ cm) using the parallel-resistor model. However, this value is a bit higher than the average ρ_{sat} ($\approx$ 165 $\mu\Omega$ cm) obtained from the ion-displacement model. It was mentioned earlier at the end of Sec. IV A how ρ_{sat} was estimated from the extrapolation of the plot of TCR vs ρ (Fig. 4) to TCR=0, giving the value of $\rho_{sat} \approx 180$ $\mu\Omega$ cm. This agreement is very satisfying since the value of ρ_{sat} is found here by mere extrapolation of the experimental data independent of any model. Thus the values of ρ_{sat}, derived from our experiments using the parallel-resistor and the ion-displacement models, are more or less in good agreement with the theoretical value obtained from Eq. (12) in this system of disordered alloys.

The values of the electron-phonon scattering term D in the ion-displacement model are found in the range (0.12–0.16) $\mu\Omega$ cm K^{-1} as given in Table IV. In the high-temperature limit, the form of $\rho_{ph}(T)$ in Eq. (5) of the parallel-resistor model reduces to βT where $\beta = B/(2\Theta_D)$ in Eq. (1) of Wilson model[32] for transition metals. Substituting $\Theta_D = 400$ K and the values of B from Table III, we get β in the range of (0.25–0.40) $\mu\Omega$ cm K^{-1}. With alloying the density of states [$N(E_F)$] at the Fermi level (E_F), the Fermi velocity (v_F) and the electron-phonon coupling constant (λ_{tr}) are not expected to vary significantly. Therefore, it is possible to estimate β, at least roughly, in our alloys employing the theoretical[10,11] relation

$$\beta = \left[\frac{6\pi k_B \lambda_{tr}}{\hbar N(E_F)\langle v_F\rangle^2 e^2}\right], \tag{13}$$

where k_B is the Boltzmann constant and $\hbar$ Planck's constant. As we have mentioned earlier, to the best of our knowledge there is no band theory calculation available for these systems of ternary $3d$ transition-metal alloys. It is therefore difficult to estimate β from Eq. (13). Nevertheless, we have attempted to estimate β using $N(E_F) \approx 14$ states/eV/unit

cell as found from the low-temperature specific heat measurements in the temperature range of 4.2–45 K on similar FeNiCr alloys (concentrations are not exactly alike) by Pecherskaya *et al.*[43] We have used the value of the transport electron-phonon coupling constant $\lambda_{tr}=0.6$ obtained from a different work of the same authors.[46] Substituting all these values in Eq. (13) one obtains $\beta \approx 0.02\ \mu\Omega\ \mathrm{cm\ K^{-1}}$. This value is roughly 10 times smaller than those obtained from the parallel-resistor ($B/2\Theta_D$) and the ion-displacement (D) models. Although this theoretical estimate of β is very crude due to the lack of knowledge of the band structure, its value is not too far from those derived from our electrical transport measurements.

We have also compared the values of ρ_{sat} ($\approx$ 200 $\mu\Omega$ cm) obtained from our experiments with the theoretical value when these metallic systems approach Mott's minimum metallic conductivity[41] regime (near to the metal-insulator transition). Mott has always made a distinction between the two situations, namely, conductivity σ when the electron mean free path approaches the lattice spacing ($l \sim a$) and the minimum metallic conductivity (as seen in different metal oxides). As mentioned earlier, Gurvitch[14] has shown that σ_{sat} ($\approx \rho_{sat}^{-1}$) is always larger than σ_{min} ($\approx 0.026e^2/\hbar a$, the minimum metallic conductivity) and has given a relationship between them [Eq. (7)]. We have estimated σ_{min} using $a=3.58$ Å (e and $\hbar$ being constants) and find that our $\sigma_{sat} \approx 25\sigma_{min}$. We have also evaluated the same factor from Eq. (7) using $n=6\times10^{22}/\mathrm{cm}^3$ (Ref. 45) and $a=3.58$ Å and find that it is 20 and not 25. Thus for the alloys under investigation, in the saturation regime ($l \sim a$), the conductivity is still much higher and is not at all close to Mott's minimum metallic conductivity (σ_{min}) regime. This observation supports Gurvitch's argument.[14]

V. CONCLUSIONS

We have performed systematic electrical resistivity measurements on γ-$Fe_{80-x}Ni_xCr_{20}$ ($14 \leqslant x \leqslant 30$) substitutionally disordered, crystalline, magnetic alloys. In the high-temperature region ($T > 200$ K) we observe a noticeable downward deviation of ρ from a linear temperature dependence. This is an indication of resistivity saturation in all these alloys independent of their low-temperature magnetic states in sharp contrast to the linearity of $\rho(T)$ continuing even up to 300 K, as reported by Banerjee and Raychaudhuri.[28] Our study provides a rigorous test of all the theoretical models. In conclusion, we argue that the particular way in which the alloys approach saturation can be understood quite well on the basis of the parallel-resistor model. The phonon-ineffectiveness model has failed to explain this strong downward DFL of ρ at high temperatures, at least in our alloys. The ion-displacement model also provides a consistent explanation of the DFL of ρ at high temperatures. However, every model has its limitations. None of them provide a single constant saturation resistivity derived from the experimental data. One also does not know whether a unique saturation resistivity or a number of them is desirable for the entire range of concentration (x) of this particular alloy system because of insufficient theoretical inputs. Further, we conclude that the σ_{sat} in these alloys are much higher than those expected if this system approaches the minimum metallic conductivity region (σ_{min}). Thus the two situations, namely, the conductivity σ when the electron mean free path approaches the lattice spacing ($l \approx a$) and the minimum metallic conductivity, are not alike. Greater attention should be paid in the direction of the band theory calculations in ternary $3d$ transition-metal alloys which ultimately will help in understanding the transport properties of these systems in a more quantitative manner. At low temperatures, we conclude that the T^2 dependence of ρ of these magnetic alloys in the long-range (FM or AFM) regime mainly arises from the electron-magnon (spin-wave) scattering. The latter also provides a more consistent picture for the entire range of x. We also find that the Baber mechanism is too small to explain this low-temperature T^2 behavior. We further conclude that for the alloys ($x=19$ and 21) in the SG regime, the T^2 contribution becomes somewhat smaller (as it should be) and an additional T^3 contribution, which arises from the electron-phonon scattering in the presence of an s-d interaction, plays an important role in the behavior of the low-temperature $\rho(T)$.

ACKNOWLEDGEMENTS

We would like to thank Dr. K. P. Rajeev for many useful discussions and G. C. John and Professor R. C. Budhani for a careful reading of the manuscript. Financial assistance from Project No. SP/S2/M-45/89 of the Department of Science and Technology, Government of India, is gratefully acknowledged.

[1] P. A. Lee and T. V. Ramakrishnan, Rev. Mod. Phys. **57**, 287 (1985).
[2] A. F. Ioffe and A. R. Regel, Prog. Semicond. **4**, 237 (1960).
[3] J. H. Mooij, Phys. Status Solidi A **17**, 521 (1973).
[4] B. L. Altshuler and A. G. Aronov, in *Electron-Electron Interactions in Disordered Systems*, edited by A. L. Efros and M. Pollak (North-Holland, Amsterdam, 1985).
[5] Z. Fisk and G. W. Webb, Phys. Rev. Lett. **36**, 1084 (1976).
[6] H. Wiessmann, M. Gurvitch, H. Lutz, A. K. Ghosh, B. Schwarz, M. Strongin, P. B. Allen, and J. W. Halley, Phys. Rev. Lett. **38**, 782 (1977).
[7] K. Ghosh, S. Ramakrishnan, and Girish Chandra, Phys. Rev. B **48**, 10 440 (1993).
[8] S. Ramakrishnan, K. Ghosh, and Girish Chandra, Phys. Rev. B **46**, 2958 (1992).
[9] P. J. Cote and K. V. Meisel, Phys. Rev. Lett. **40**, 1586 (1978).
[10] P. B. Allen, W. E. Pickett, K. M. Ho, and M. L. Cohen, Phys. Rev. Lett. **40**, 1532 (1978).
[11] B. Chakraborty and P. B. Allen, Phys. Rev. Lett. **42**, 736 (1979).
[12] R. B. Laughin, Phys. Rev. B **26**, 3479 (1982).
[13] M. Gurvitch, Phys. Rev. B **24**, 7404 (1981).
[14] M. Gurvitch, Phys. Rev. B **28**, 544 (1983).

[15] A. Ron, B. Shapiro, and M. Weger, Philos. Mag. B **54**, 553 (1986).
[16] M. Gurvitch, A. K. Ghosh, B. L. Gyorffy, H. Lutz, O. F. Kammerer, J. S. Rosner, and M. Strongin, Phys. Rev. Lett. **41**, 1616 (1978).
[17] J. A. Wollam and S. A. Alterovitz, Phys. Rev. B **19**, 749 (1979).
[18] J. J. Lin, C. Yu, and Y. D. Yao, Phys. Rev. B **48**, 4864 (1993).
[19] J. A. Mydosh, P. J. Ford, M. P. Kawatra, and T. E. Whall, Phys. Rev. B **10**, 2845 (1974).
[20] A. Banerjee and A. K. Majumdar, Phys. Rev. B **46**, 8958 (1992).
[21] S. Senoussi and Y. Öner, Phys. Rev. B **28**, 455 (1983).
[22] H. Z. Durusoy and Y. Öner, Phys. Rev. B **42**, 6831 (1990).
[23] A. K. Majumdar and P. v. Blanckenhagen, Phys. Rev. B **29**, 4079 (1984).
[24] A. K. Majumdar and P. v. Blanckenhagen, J. Magn. Magn. Mater. **40**, 227 (1983).
[25] T. K. Nath and A. K. Majumdar, J. Appl. Phys. **70**, 5828 (1991).
[26] M. Gabay and G. Toulouse, Phys. Rev. Lett. **47**, 201 (1981).
[27] S. Banerjee and A. K. Raychaudhuri, Solid State Commun. **83**, 1047 (1992).
[28] S. Banerjee and A. K. Raychaudhuri, Phys. Rev. B **50**, 8195 (1994).
[29] J. M. Ziman, *Electrons and Phonons* (Oxford University Press, London, 1963).
[30] G. T. Meaden, *Electrical Resistance of Metals* (Plenum Press, New York, 1965).
[31] J. S. Dugdale, *The Electrical Properties of Metals and Alloys*, Vol. 5 of *The Structures and Properties of Solids* (Edward Arnold, London, 1977).
[32] A. H. Wilson, Proc. R. Soc. London A **167**, 580 (1938).
[33] G. K. White and S. B. Woods, Philos. Trans. R. Soc. London A **251**, 273 (1959).
[34] E. A. Turov, Izv. Akad. Nauk SSSR, Ser. Fiz. **19**, 426 (1955).
[35] T. Kasuya, Prog. Theor. Phys. (Kyota) **16**, 58 (1956).
[36] T. Kasuya, Prog. Theor. Phys. (Kyota) **22**, 227 (1959).
[37] I. Mannari, Prog. Theor. Phys. (Kyota) **22**, 335 (1959).
[38] D. A. Goodings, Phys. Rev. B **132**, 542 (1963).
[39] W. G. Baber, Proc. R. Soc. London A **158**, 383 (1937).
[40] J. Appel, Phys. Rev. **125**, 1815 (1962); Philos. Mag. **8**, 1071 (1963).
[41] N. F. Mott, *Metal-Insulator Transition* (Taylor & Francis, London, 1974); Philos. Mag. B **44**, 265 (1981).
[42] A. Ron, B. Shapiro, and M. Weger, Philos. Mag. B **54**, 553 (1986).
[43] V. I. Pecherskaya, D. N. Bolshutkin, A. V. Butenko, V. N. Beilinson, V. I. Ovcharenko, V. A. Pervakov, and N. Yu. Tyutryumova, Sov. J. Low Temp. Phys. **14**, 505 (1988).
[44] C. Y. Wu and J. J. Lin, Z. Phys. B **93**, 269 (1994).
[45] S. Banerjee, Ph.D. thesis, Indian Institute of Science, Bangalore, India, 1993.
[46] V. I. Pecherskaya, A. V. Butenko, and D. N. Bolshutkin, Fiz. Nizk. Temp. **13**, 1146 (1987) [Sov. J. Low Temp. Phys. **13**, 648 (1987)].